Assessing canopy PRI for water stress detection with diurnal airborne imagery

L. Suárez [a], P.J. Zarco-Tejada [a,*], G. Sepulcre-Cantó [a], O. Pérez-Priego [a], J.R. Miller [b], J.C. Jiménez-Muñoz [c], J. Sobrino [c]

[a] Instituto de Agricultura Sostenible (IAS), Consejo Superior de Investigaciones Científicas (CSIC), Córdoba, Spain
[b] Department of Earth and Space Science and Engineering, York University, Toronto, Canada
[c] Global Change Unit, Department of Thermodynamics, Faculty of Physics, University of Valencia, Valencia, Spain

Abstract

A series of diurnal airborne campaigns were conducted over an orchard field to assess the canopy *Photochemical Reflectance Index* (PRI) as an indicator of water stress. Airborne campaigns over two years were conducted with the *Airborne Hyperspectral Scanner* (AHS) over an orchard field to investigate changes in PRI, in the *Transformed Chlorophyll Absorption in Reflectance Index* (TCARI) normalized by the *Optimized Soil-Adjusted Vegetation Index* (OSAVI) (TCARI/OSAVI), and in the *Normalized Difference Vegetation Index* (NDVI) as function of field-measured physiological indicators of water stress, such as stomatal conductance, stem water potential, steady-state fluorescence, and crown temperature. The AHS sensor was flown at three times on each 2004 and 2005 years, collecting 2 m spatial resolution imagery in 80 spectral bands in the 0.43–12.5 µm spectral range. Indices PRI, TCARI/OSAVI, and NDVI were calculated from reflectance bands, and thermal bands were assessed for the retrieval of land surface temperature, separating pure crowns from shadows and sunlit soil pixels. The *Photochemical Reflectance Index*, originally developed for xanthophyll cycle pigment change detection was calculated to assess its relationship with water stress at a canopy level, and more important, to assess canopy structural and viewing geometry effects for water stress detection in diurnal airborne experiments. The FLIGHT 3D canopy reflectance model was used to simulate the bi-directional reflectance changes as function of the viewing geometry, background and canopy structure. This manuscript demonstrates that the airborne-level PRI index is sensitive to the de-epoxidation of the xanthophyll pigment cycle caused by water stress levels, but affected diurnally by the confounding effects of BRDF. Among the three vegetation indices calculated, only airborne PRI demonstrated sensitivity to diurnal changes in physiological indicators of water stress, such as canopy temperature minus air temperature (Tc–Ta), stomatal conductance (G), and stem water potential (ψ) measured in the field at the time of each image acquisition. No relationships were found from the diurnal experiments between NDVI and TCARI/OSAVI with the tree-measured physiological measures. FLIGHT model simulations of PRI demonstrated that PRI is highly affected by the canopy structure and background.
© 2007 Elsevier Inc. All rights reserved.

Keywords: Water stress; Thermal; Hyperspectral; PRI; TCARI/OSAVI; Airborne; TES; AHS; Remote sensing

1. Introduction

The *Photochemical Reflectance Index* (PRI) is a physiological reflectance index sensitive to the de-epoxidation state of the xanthophyll cycle pigments and the efficiency of photosynthesis (Gamon et al., 1992). The xanthophyll cycle is associated with diurnal reductions in photosynthetic efficiency, as the xanthophyll cycle pigment violaxanthin is de-epoxidized under conditions of excess light since this reaction is readily reversed under limiting light (Gamon et al., 1992). Thus, the de-epoxidation state, or in other words, the concentration of the three xanthophyll cycle pigments, may be used as an indicator of *short-term* changes in photosynthetic activity. Several studies focus the assessment of PRI at the leaf level to track

* Corresponding author. Instituto de Agricultura Sostenible (IAS), Consejo Superior de Investigaciones Científicas (CSIC), Alameda del Obispo, s/n 14004-Córdoba, Spain. Tel.: +34 957 499 280, +34 676 954 937; fax: +34 957 499 252.
 E-mail address: pzarco@ias.csic.es (P.J. Zarco-Tejada).
 URL: http://www.ias.csic.es/pzarco (P.J. Zarco-Tejada).

photosynthesis changes as function of elevation and latitude (Richardson & Berlyn, 2002; Richardson et al., 2003), and across ecosystems with nutrient level variability (Whitehead et al., 2005). Photosynthetic light-use efficiency (LUE) was demonstrated to be successfully estimated with PRI (Serrano & Peñuelas, 2005), although effects due to the species were found on leaf PRI (Guo & Trotter, 2004), as well as inconsistencies in the PRI/LUE relationship as function of drought conditions (Sims et al, 2006). The relationships between PRI and chlorophyll fluorescence measures have also been the focus of increasing interest in recent research. Relationships between PRI and dark-adapted fluorescence (Fv/Fm) over seasonal trials were demonstrated (Weng et al., 2006a,b), and the assessment for leaf-level PRI sensitivity to seasonal changes were studied for parameters such as LUE (Nakaji et al., 2006), carbon uptakes (Filella et al., 2004), carotenoid pigments and photosynthetic activity (Stylinski et al., 2002), and carotenoid/total chlorophyll ratio (Sims & Gamon, 2002).

Nevertheless, difficulty is encountered in the assessment of PRI at canopy scale related with the effects of the structure and viewing geometry on the vegetation reflectance index. Some successful studies with field spectrometers at the canopy scale in diurnal cycles and seasonal acquisitions demonstrated that PRI is sensitive to photosynthetic efficiency (Nichol et al., 2006), under nutrient stress conditions (Strachan et al., 2002; Trotter et al., 2002), and over the *green-up* period in a boreal forest (Nichol et al., 2002). Filella et al. (1996) showed that PRI was significantly correlated with de-epoxidation state, zeaxanthin concentration, and with photosynthetic radiation-use efficiency on a cereal canopy. In addition, canopy-level relationships between PRI and chlorophyll fluorescence (Louis et al., 2005) suggested the potential estimation of carbon assimilation at canopy level using the PRI index. Although several studies demonstrate the sensitivity of PRI bands to the de-epoxidation state, which is potentially affected by water stress conditions, limited work has been found which demonstrate that PRI tracks the diurnal dynamics of water-limited physiology. Thenot et al. (2002) and Winkel et al. (2002) demonstrated the sensitivity of PRI to water stress conditions, although structural effects caused by the water stress would also affect the reflectance signal. The
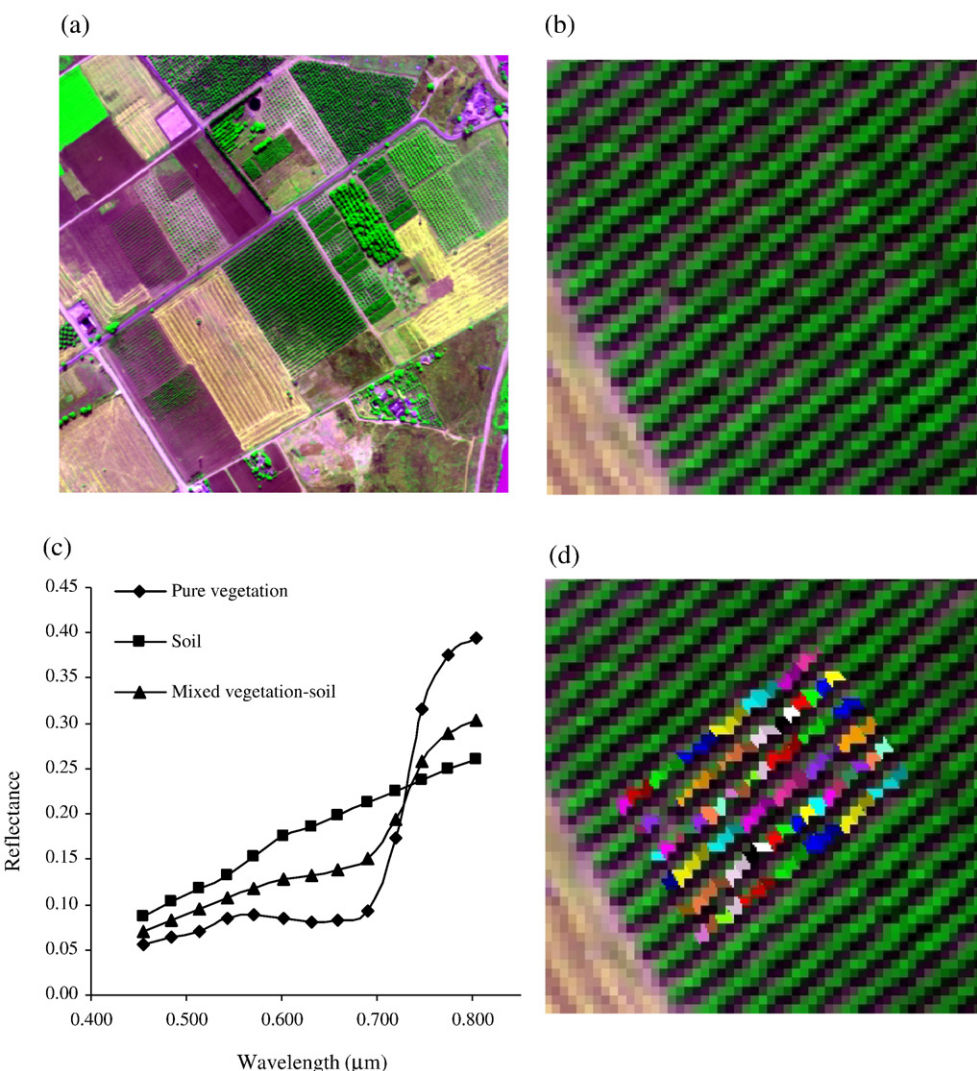

Fig. 1. Overview of the area acquired with the AHS instrument (a). Detail of the olive orchard where the experiment was conducted (b). AHS spectra for pure vegetation, soil and mixed vegetation-soil pixels (c). Regions of interest created for single tree crowns (d).

relationships obtained at canopy level between PRI and chlorophyll fluorescence under water stress conditions (Dobrowski et al., 2005; Evain et al., 2004) demonstrated that PRI accurately tracked induced stress conditions.

However, consistent relationships between PRI, radiation-use efficiency and chlorophyll fluorescence measures at the canopy level have not always been found. Furthermore, the application of PRI at larger scales would present additional complications due to heterogeneous landscape composition, atmospheric interference and background effects. Accordingly, a number of formulations for PRI have been proposed in the literature using different reference wavelengths to minimize diurnal sun angle effects (Filella et al., 1996; Gamon et al., 1992; Peñuelas et al., 1994). These undesired effects of canopy structure, viewing geometry and background on PRI may be an important reason for the limited work published from airborne- and satellite-level research on PRI. Examples are limited to the *Airborne Visible Infrared Imaging Spectrometer* (AVIRIS) for carbon and water vapor flux estimations using PRI, NDVI and PWI (Fuentes et al., 2006), satellite level using Hyperion for LUE estimations (Asner et al., 2005), and MODIS-derived PRI for inter-annual variations in LUE (Drolet et al., 2005).

Although PRI has been successfully applied for the remote sensing of photosynthetic processes at the leaf (Gamon et al., 1997; Tambussi et al. 2002) and at the canopy levels (Evain et al. 2004; Fuentes et al. 2006; Louis et al. 2005; Nichol et al. 2000; Peñuelas & Inoue 2000; Rahman et al. 2004), questions still need to be answered regarding the interpretation of PRI inter-specific and long-term dynamics changes (Gamon & Surfus, 1999; Guo & Trotter 2004; Weng et al., 2006a). Effects due to the canopy architecture, canopy structure, background and the viewing geometry at the time of image acquisition are key factors inhibiting successful understanding of PRI changes. Work by Barton and North (2001) demonstrated that PRI is highly affected by the view angle, highly influenced by soil background at canopies with LAI <3, and also affected by the leaf angle distribution function at large view angles. The present study presents new insights on the understanding of the diurnal dynamics of canopy PRI as a function of water stress as imaged by an airborne sensor that enabled tree crowns to be targeted over the course of diurnal airborne campaigns. Relationships with image-extracted canopy temperature and field-measured fluorescence are also discussed, along with the assessment of diurnal effects of the viewing geometry on the PRI index for water stress detection.

2. Methods

2.1. Field data collection

The study site is located in Córdoba, southern Spain (37.8°N, 4.8°W), an area dominated by Mediterranean climate with an annual rainfall of 650 mm concentrated between autumn to spring. Data was collected in an irrigated 4 ha-orchard established in 1997 with olive trees (*Olea europaea* L. cv. "Arbequino") in a 3.5 × 7 m grid. The soil was kept under no-tillage conditions using weed-killers. The tree lines followed a

north–south direction and the trees were planted on ridges to avoid flooding problems due to the soil-low percolation rate. Drip irrigation permitted the use of different water treatment amounts within the same field. The experiment was designed in an area of six rows with three different water treatments: (i) irrigating 2.8 mm/day (well-irrigated treatment used as reference, treatment R), (ii) 0.7 mm/day (deficit treatment S1), and (iii) combining a deficit irrigation (1.2 mm/day) with intermittent application from 14 June 2004 to 5 July and from 6 September to 19 October of the same year (deficit treatment S2). A more detailed description of this experiment and study site for water stress can be found in Pérez-Priego et al. (2005) (related to fluorescence detection using a high spectral resolution spectrometer), and Sepulcre-Cantó et al. (2006) (related to thermal detection).

Thermal data were taken continuously on ten trees comprising the three irrigation treatments. The instruments used were IRTS-P sensors (Apogee, UT, USA) positioned 1 m over the monitored trees recording in the 6.5–14 μm range. Three data-loggers (model CR10X, Campbell Sci., UT, USA) were used to record the mean temperature every five minutes out of 300 measurements in each interval (1 s^{-1}). At the same time, temperature over a water body was measured with a field thermal radiometer (model Raynger II, Raytek, CA, USA) with a single broadband sensor covering the range 8–14 μm. In addition, air temperature data was collected at image acquisition times with a Vaisala Weather Transmitter (model WXT510, Vaisala Oyj, Helsinki, Finland) installed 1 m over a well-irrigated tree in the study site. Relative temperature was calculated as the difference between the temperature of the crowns of the trees and the air temperature at the same time (Tc–Ta).

A Pulse-Amplitude-Modulated Fluorometer (PAM-2100, Heinz Walz GMBH, Effeltrich, Germany) was used to measure leaf steady-state chlorophyll fluorescence (Ft). The measurements were taken on an average of fifty exposed leaves per tree five times per day from 6:30 to 11:30 solar time between June and
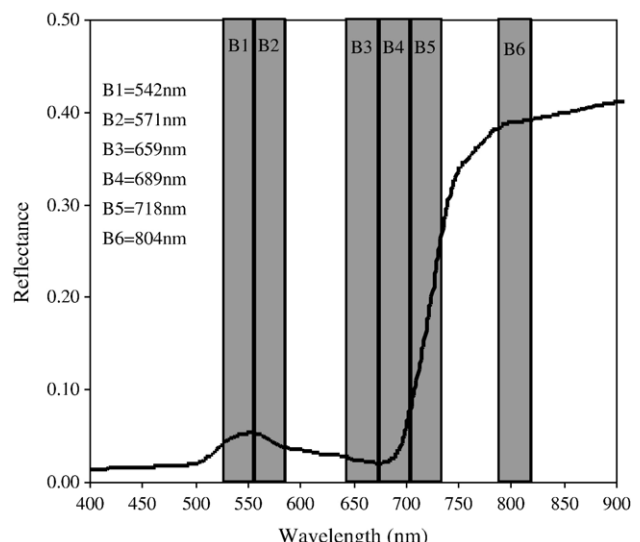

Fig. 2. Center wavelength and bandwidth for the AHS bands used to calculate the vegetation indices NDVI (B6 and B3), TCARI/OSAVI (B1, B4, B5 and B6) and PRI (B1 and B2).

November 2004. The PAM-2100 standard procedure was used to obtain steady-state fluorescence (Ft) and effective quantum yield ($\Delta F/Fm' = (Fm' - Ft)/Fm'$) at the leaf level. Stomatal conductance (G) was measured once a week at hourly intervals from 7:30 to 11:30 GMT on one tree per irrigation treatment. The instrument used was a leaf steady-state porometer (model PMR4, PP Systems, Hitchin Herts, Great Britain). Stem water potential (Ψ) was monitored weekly with a Scholander pressure bomb (PWSC Model 3000, Soil Moisture Equipment Corp., California) on four trees from each S1 and S2 deficit irrigation treatments, and on three trees under the well-irrigated R treatment. The former eleven trees used for the detailed monitoring were located in the centre of treatment blocks to avoid edge influences. Water potential measurements were taken at 10:00 GMT on two shaded leaves near the trunk. The field measurements were collected on individual trees, conducting the further analysis both at the tree and block levels. Both thermal data and reflectance indices for stress detection analysis were then extracted from the multi-year airborne campaign acquired diurnally over the study site.

Fig. 4. Model simulations conducted with FLIGHT for a forest canopy (a) and a crop canopy planted in regular grids (b). Input parameters for the forest canopy (a) were total LAI=1.7, fraction cover=0.8, leaf size=1.5, fraction of green leaves=0.85, fraction of bark=0, crown shape=spherical, soil roughness=0, aerosol optical thickness=0.15, solar zenith=21.36°, solar azimuth=294.44°, view zenith=0°, view azimuth=0°. Parameters for the crop canopy (b) comprised a total LAI=0.8, fraction cover=0.8, tree LAI=1, leaf size=2, fraction of green leaves=0.85, fraction of bark=0, LAD=spherical, crown shape=spherical, crown radius=1.5, tree height=4, soil roughness=0, aerosol optical thickness=0.15, solar zenith=21.36°, solar azimuth=20.94°, view zenith=0°, view azimuth=0°.

2.2. Airborne image acquisitions

Two airborne campaigns were conducted over the experimental field to acquire six images corresponding to three flight times (7:30, 9:30 and 12:30 GMT) on two consecutive years (25th July 2004 and 16th July 2005). Therefore, two complete data sets comprising field physiological measures and airborne thermal and reflectance imagery were acquired for further analysis of water stress detection. The airborne campaigns were conducted in collaboration with the Spanish Aerospace Institute (INTA) using the Airborne Hyperspectral Scanner (AHS) developed by Sensytech Inc. (Argon St. Inc., USA). The flight height was set to 1000 m above ground level, acquiring imagery with a 90° field of view (FOV) and 2.5 mrad instantaneous FOV, produced a spatial resolution of 2 m. In the 2004 campaign, imagery was collected at 38 bands over the 0.430–
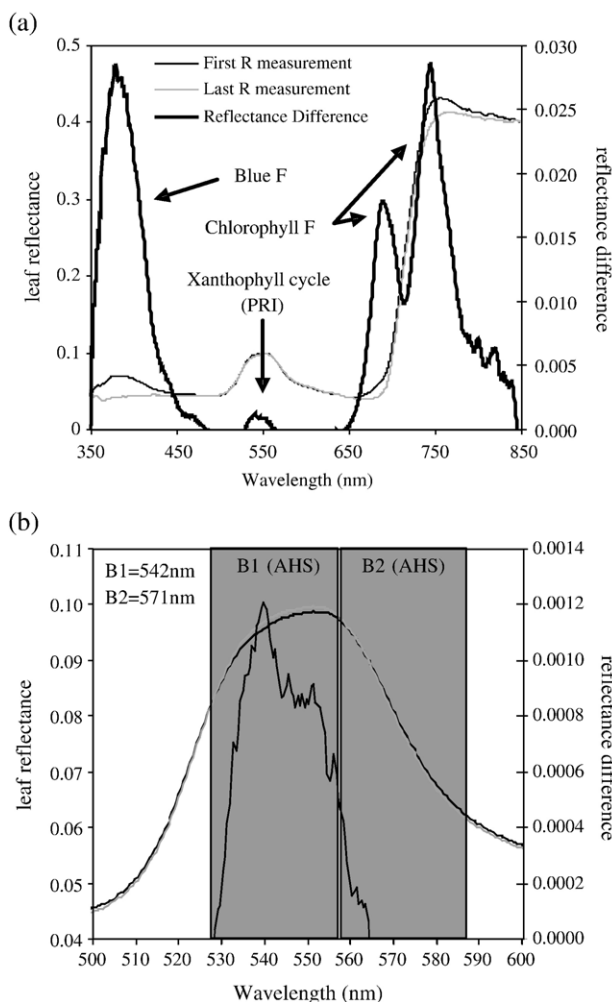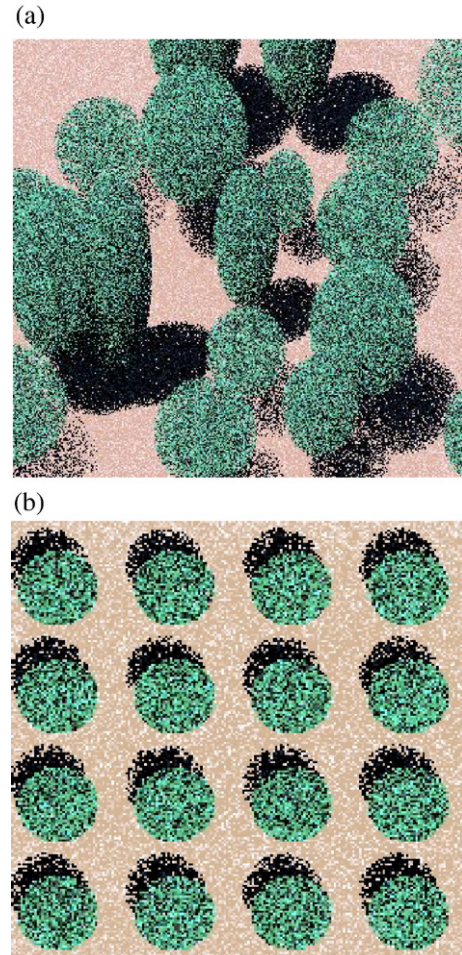

Fig. 3. (a) Leaf reflectance of dark adapted leaves (dotted line, first measurement) and under steady-state condition (continuous line, last measurement), showing the reflectance difference associated with blue fluorescence, chlorophyll fluorescence and xanthophylls pigment cycle. Changes in the PRI region are shown (b), indicating the AHS bands used in this study.

1.550 μm and 8.20–12.70 μm spectral regions. In the 2005 campaign, 80 bands were available in the 0.430–2.49 μm and 8.20–12.70 μm ranges. Atmospheric correction was conducted with the MODTRAN–4 radiative transfer code (Berk et al., 1999) supported by *in situ* radiosoundings launched at 7:00 and 12:00 GMT on 16 July 2005. Water vapour was obtained by scaling to an altitude of 1 km the measured value at the 'El Arenosillo' site, part of the AERONET network (http://aeronet.gsfc.nasa.gov). A full description of the calibration of the AHS bands and the radiometric and the atmospheric correction methodology can be found in Sobrino et al. (2006). For the VIS-SWIR region, soil reflectance spectra were used to conduct *flat-field* calibration (Ben-Dor & Levin, 2000) after atmospheric correction with MODTRAN, which compensated for residual effects on derived surface reflectance estimations in atmospheric water and oxygen absorption spectral regions (Haboudane et al., 2004; Zarco-Tejada et al., 2004). Fig. 1 shows a sample image acquired over the study site with the AHS airborne sensor after atmospheric correction (Fig. 1a), a subset of the entire imagery (Fig. 1b), and the corresponding spectra extracted from the imagery for the three scene components: i) pure tree crowns; ii) pure soil spectra, and iii) mixed pixels comprising pure crown, soil and shadow scene components (Fig. 1c). The

extraction of pure crown pixels was conducted with the 2 m spatial resolution imagery (Fig. 1d shows the identification of single crowns) enabling the calculation of indices without the effects of shadow and soil components.

Vegetation indices were calculated from each of the six available images to track changes in canopy structure and pigment concentration as function of the water stress status. The *Normalized Difference Vegetation Index* (NDVI) (Rouse, 1974) was calculated in this study to track changes in canopy structure in healthy vegetation, due to its relationship with leaf area index. The *Transformed Chlorophyll Absorption in Reflectance Index* (TCARI) (Haboudane et al., 2002) based on the *Modified Chlorophyll Absorption in Reflectance* (MCARI) (Daughtry et al., 2000), normalized by the *Optimized Soil-Adjusted Vegetation Index* (OSAVI) (Rondeaux et al., 1996) to obtain TCARI/OSAVI have been demonstrated to successfully minimize soil background and leaf area index variation in crops, providing predictive relationships for chlorophyll concentration estimation with hyperspectral imagery in closed crops (Haboudane et al., 2002) and open tree canopy orchards (Zarco-Tejada et al., 2004). Finally, the *Photochemical Reflectance Index* (PRI), originally developed for xanthophyll cycle pigment change detection (Gamon et al., 1992) and suggested as a potential indicator for carotenoid/chlorophyll ratio monitoring (Sims & Gamon, 2002; Zarco-Tejada et al., 2005), was calculated to assess its relationship with water stress at canopy levels, and more important, to assess canopy structural and viewing geometry effects for water stress detection in diurnal airborne experiments. The three indices are described in Eqs. (1)–(3).

$$NDVI = \frac{R_{800} - R_{670}}{R_{800} + R_{670}} \qquad (1)$$

TCARI/OSAVI
$$= \frac{3^*[(R_{700} - R_{670}) - 0.2^*(R_{700} - R_{550})^*(R_{700}/R_{670})]}{(1 + 0.16)^*(R_{800} - R_{670})/(R_{800} + R_{670} + 0.16)} \qquad (2)$$

$$PRI = \frac{R_{570} - R_{531}}{R_{570} + R_{531}}. \qquad (3)$$

Adapted indices with spectral bands as available from the AHS airborne sensor were 659 nm and 804 nm for NDVI; 542 nm, 689 nm, 718 nm and 804 nm for TCARI/OSAVI; and 542 nm and 571 nm for PRI (all of them with 29 nm FWHM). Fig. 2 shows the centre wavelength and bandwidths for the spectral bands used in this study to calculate the vegetation indices NDVI, TCARI/OSAVI and PRI. The feasibility of the AHS airborne sensor for PRI index changes associated with the de-epoxidation of the xanthophyll pigment cycle was further assessed. The 29 nm FWHM bandwidth of the two bands used for PRI calculation from the AHS sensor was compared with previous laboratory studies conducted which focused on the detection of fluorescence effects on leaf and canopy reflectance (Zarco-Tejada et al., 2000).

Table 1
Nominal values and range of parameters used for leaf and canopy modelling with PROSPECT and FLIGHT for the orchard study sites

	Units/values used
Leaf optical and structural parameters	
Hemispherical reflectance and transmittance of green leaves	Measured
Hemispherical reflectance and transmittance of senescent leaves	Not used
Leaf equivalent radius	cm
Canopy layer and structural parameters	
Leaf area index of vegetation	1–5 m²/m²
Total leaf area index	m²/m²
Fractional cover	0–1
Leaf angle distribution	9 parameters
Fraction of green leaves	0.85
Fraction of senescent leaves	0
Fraction of bark	0.15
Hemispherical reflectance and transmittance of bark	Measured
Number of stands and position coordinates	Coordinates (m)
Crown shape	Spherical
Crown height and radius	m
Trunk height and radius	m
Background and viewing geometry	
Solar zenith and azimuth	degrees
Instrument zenith and azimuth	degrees
Soil reflectance	Image extracted
Soil roughness	0–1
Aerosol optical thickness (AOD)	0.15

Canopy structural parameters were used in the FLIGHT model for simulation of the canopy reflectance by radiative transfer. Leaf structural parameters, and leaf biochemical parameters were used for leaf-level simulation of reflectance and transmittance using PROSPECT.

Reflectance difference calculations from dark adapted leaves and under steady-state condition (Fig. 3a, adapted from Zarco-Tejada et al., 2000) enabled the emission bandwidths associated with blue fluorescence, chlorophyll fluorescence, and de-epoxidation of the xanthophyll pigment cycle later used to develop the PRI index to be studied. The bandwidth of the spectral region sensitive to the xanthophyll pigment is shown to be 26 nm FWHM, and centered on the 542 nm band in the AHS sensor (Fig. 3b).
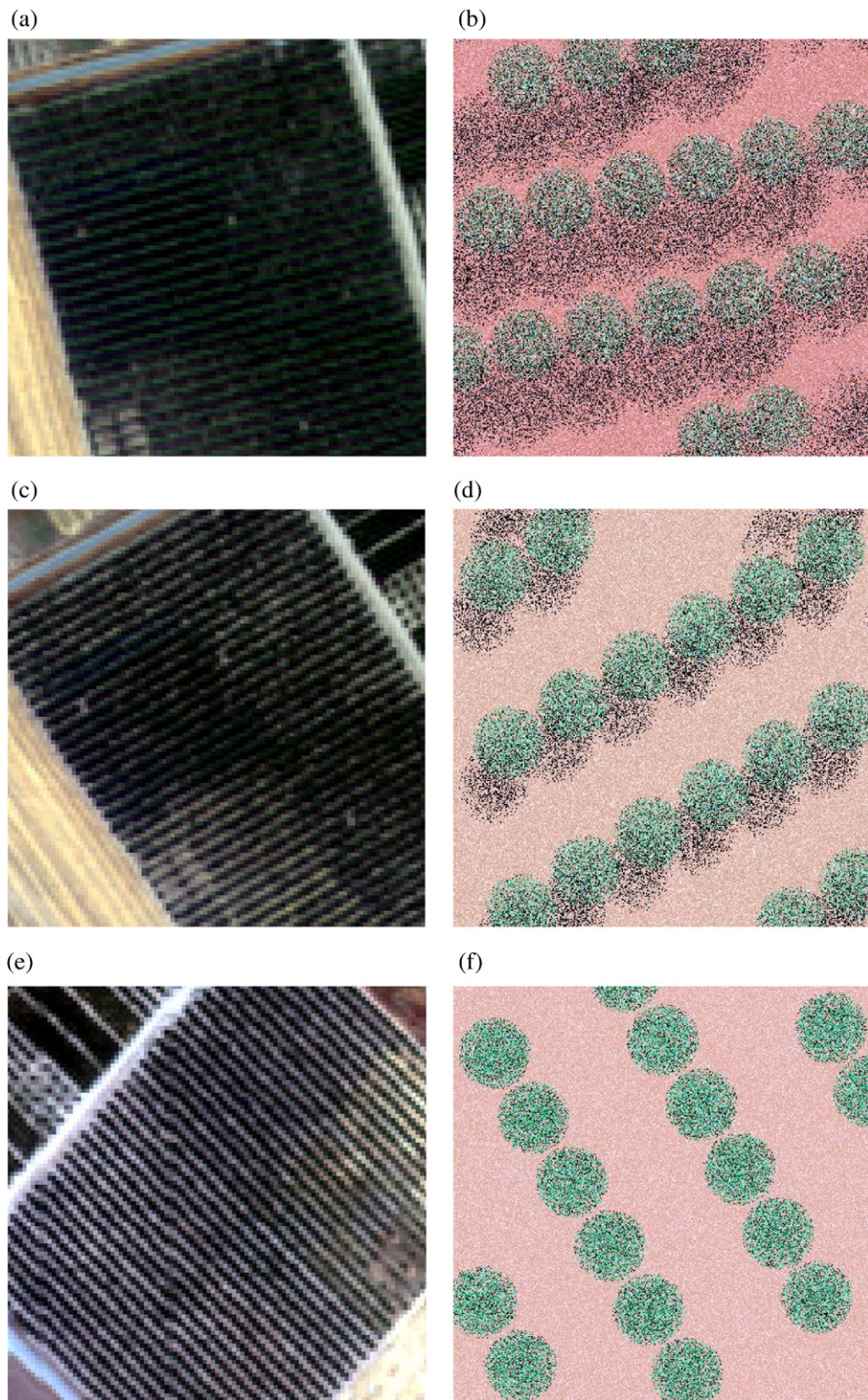

Fig. 5. AHS images acquired from the study site showing the corresponding simulations conducted with FLIGHT at 7:30 GMT (a, b), 9:30 GMT (c and d) and 12:30 GMT (e and f). Input parameters were the total LAI=0.39, fractional cover=0.39, crown LAI=1, leaf size=1.26, fraction of green leaves=0.85, fraction of bark=0, LAD=spherical, crown shape=spherical, crown radius=1.75 m, tree height=3.45 m, soil roughness=0, aerosol optical thickness=0.1, view zenith=0°, view azimuth=0°, solar azimuth=160°, solar zenith=58.29° (b), 36.19° (d), 0° (f).
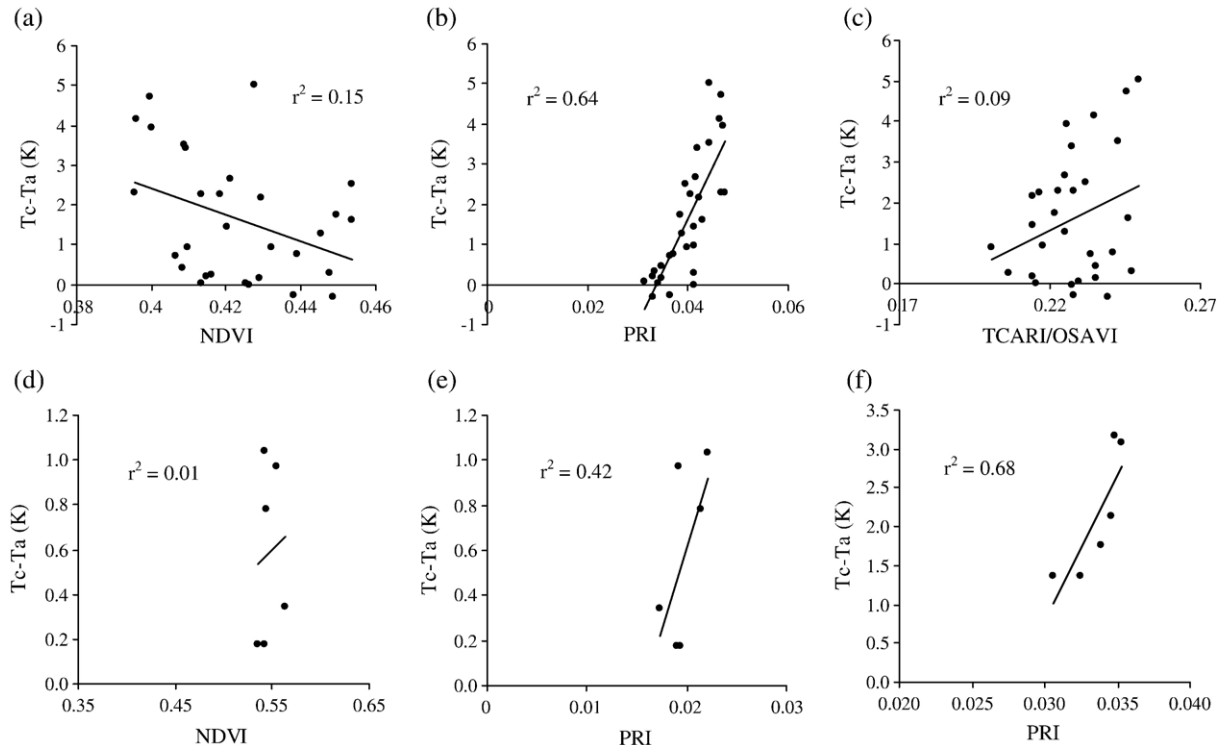
Fig. 6. Relationships obtained between NDVI, TCARI/OSAVI and PRI with Tc–Ta (K) at tree level (a, b and c respectively), and block level at 7:30 GMT (d and e) and 9:30 (f).

Therefore, the use of the 542 and 571 nm bands from the AHS airborne sensor for PRI calculation was considered justified. The indices were extracted for each tree and block of trees irrigated under different doses at each airborne acquisition for the three flight times. Additionally, crown and block surface temperature was retrieved from each airborne acquisition at the same 2 m
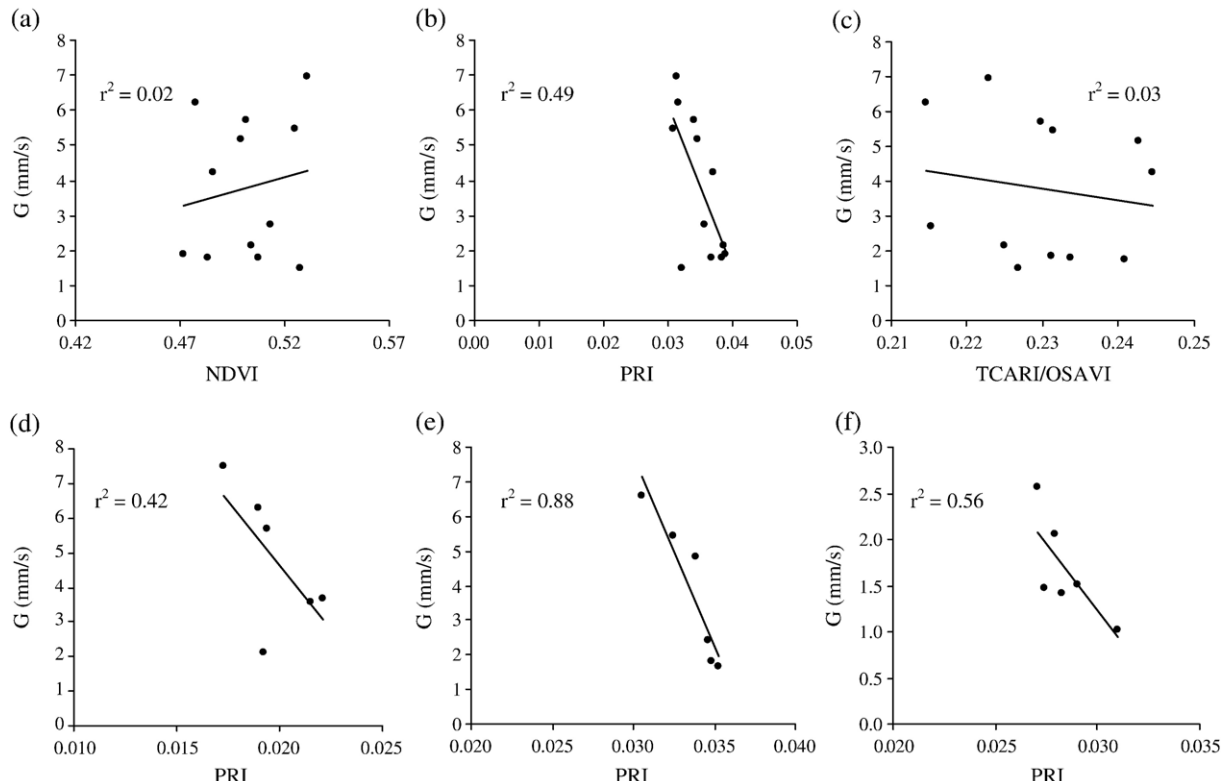

Fig. 7. Relationship between stomatal conductance (G) and NDVI (a), PRI (b) and TCARI/OSAVI (c) at tree scale at 9:30 GMT. At the block scale, the relationships found between conductance and PRI for different times of the day is presented in figures (d), (e) and (f) at 7:30 GMT, 9:30 GMT and 12:30 GMT respectively.
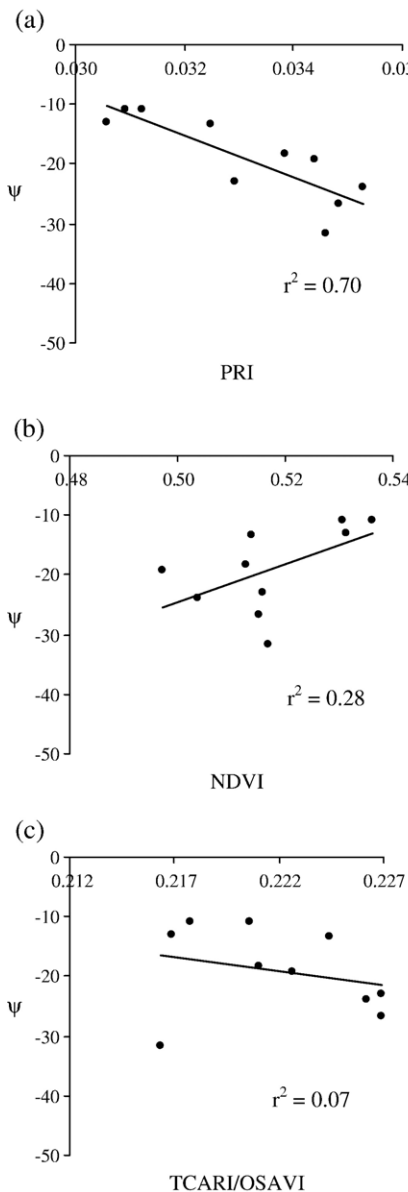
Fig. 8. Relationship between stem water potential (Ψ) and PRI (a), NDVI (b) and TCARI/OSAVI (c) at block scale at 9:30 GMT.

spatial resolution. The airborne and field datasets enabled the assessment of relationships between airborne vegetation indices, crown temperature, field water potential, stomatal conductance and steady-state fluorescence as function of diurnal effects of water stress for the 2004 and 2005 campaigns.

2.3. Simulation with FLIGHT radiative transfer model

A three dimensional forest light interaction model, FLIGHT (North, 1996) was used to simulate the radiative transfer in the canopy architecture of the study site used in this experiment. The purpose was to assess the bi-directional reflectance distribution function (BRDF) effects on the simulated vegetation indices (especially PRI) as function of the diurnal changes to the viewing geometry. FLIGHT is a computer simulation model based on a Monte Carlo ray tracing (MCRT) method. Ray tracing methods

are based on a sampling of photon trajectories within the vegetation canopies (Disney et al., 1999). The model is a hybrid geometric optical/radiative transfer approach that assumes the canopy consists of a series of regular geometric shapes placed on the ground surface in a prescribed manner. At the top of the canopy, the interaction of radiation within the vegetation depends on the contribution of several components such as leaves, stems, soil background, illumination and view properties of each canopy element, as well as on their number, area, orientation and position in space (Goel & Thompson, 2000; Koetz et al., 2005). The FLIGHT model requires foliage density, angular distribution and size determined individually for every single crown simulated (North, 1996). The FLIGHT model inputs consist of: (i) geometric characteristics: shape, height, radius, leaf angle distribution (LAD), leaf area index (LAI) and position of every single crown in the scene as well as trunk geometry, total scene size and vegetation coverage; (ii) spectral signatures: soil, green leaf, senescence leaf, bark spectra; (iii) sun and view zenith and azimuth angles; and (iv) other parameters as soil roughness, aerosol optical thickness and the number of photons simulated. The output of the model simulation is a 3D hyperspectral image with the same number of bands as the input spectral signatures. Fig. 4 shows a sample FLIGHT simulation scene corresponding to a heterogeneous forest with trees in a random position with different crown shapes and LAI values (Fig. 4a), and an orchard canopy scene simulating a tree-crop planted in a regular grid (Fig. 4b).

The FLIGHT model used in this study enabled the simulation of complex canopy scenes to understand the directional effects on narrow-band indices such as PRI, as well as to study the effects of soil background and shadows in vegetation indices proposed for water stress detection. Model simulations were conducted to assess the influence of the sun position, soil type and LAI on the three vegetation indices studied at crown and canopy levels. The input parameters sun and view azimuth, soil spectra and LAI were changed in the simulations, using structural input parameters such as crown shape and tree size collected in the field campaign. The leaf angle distribution (LAD) corresponded to the one measured by Mariscal et al. (2000) in the same olive orchard. Table 1 shows the input parameters required to run the FLIGHT model for the scenes simulated in this diurnal study, with simulations conducted for the three airborne acquisition times at 7:30, 9:30 and 12:30 GMT (Fig. 5)). Crown and block spectra were then extracted from both the AHS imagery and simulation scenes, and vegetation indices calculated for the three acquisition times. Diurnal variations of indices as compared with modelled changes as function of the viewing geometry and water stress condition were assessed.

3. Results

3.1. Experimental results

A detailed study was conducted to assess the relationships between crown-level vegetation indices calculated from the AHS imagery at different flight times (NDVI, TCARI/OSAVI, PRI) and field-measured physiological indicators of water stress, such as crown temperature minus air temperature (Tc–Ta) (Fig. 6), stomatal conductance (G) (Fig. 7), stem water potential

(ψ) (Figs. 8 and 9), and steady-state chlorophyll fluorescence (Ft) (Fig. 10).

The relationships found between Tc–Ta and the airborne vegetation indices for individual trees in the 2004 campaign (first year campaign since water stress was applied) (Fig. 6a, b and c) show that PRI tracks diurnal Tc–Ta changes as function of water stress ($r^2=0.64$) better than NDVI ($r^2=0.15$) and TCARI/OSAVI indices ($r^2=0.09$). In the second year after water stress treatments were applied (2005 campaign), structural effects were visually observable due to lower irrigation doses applied during the previous season. In this second year, NDVI and TCARI/OSAVI indices strengthened their relationship with Tc–Ta ($r^2=0.40$ and $r^2=0.43$) probably due to the mentioned structural and pigment degradation effects caused by the long-term water stress condition. The relationship between Tc–Ta and the spectral indices was also assessed on each flight time, in order to study their diurnal sensitivity. Results indicate the superior sensitivity of PRI as compared with the structurally-based NDVI, yielding (Tc–Ta vs NDVI) $r^2=0.01$ (7:30 GMT) (Fig. 6d) and $r^2=0.34$ (9:30 GMT), and (Tc–Ta vs PRI) $r^2=0.42$ (7:30 GMT) (Fig. 6e) and $r^2=0.68$ (9:30 GMT) (Fig. 6f). These results suggest that the PRI index is able to track diurnal and spatial changes in water stress as detected through crown temperature changes (a detailed analysis on the detection of water stress in orchard crops as function of airborne-derived Tc–Ta can be found in Sepulcre-Cantó et al. (2006, 2007)). The physiological rationale for finding relationships between crown temperature and water stress is well known and

suggested in several studies (Idso et al., 1978; Jackson & Pinter, 1981; Jackson et al., 1977). The use of thermal infrared instruments for stress detection have focused in the past on canopy temperature for monitoring stomatal conductance, based on the effects of water stress on stomatal closure and thermal energy dissipation pathways. Therefore the assessment of the relationships between optical vegetation indices and stomatal conductance would give a further insight on the successful tracking of physiological condition through the PRI index. Results show that conductance (G) was found to be better related to PRI than to NDVI and TCARI/OSAVI in 2004 and 2005 campaigns (results shown for 2005 campaign at 9:30 GMT at tree level in Fig. 7a, b and c, yielding $r^2=0.49$ for PRI and $r^2=0.02$ for NDVI and $r^2=0.03$ for TCARI/OSAVI). At a block scale (averaging the spectral reflectance from all trees irrigated under the same treatment), relationships were found between PRI and G at the three flight times in 2005 (7:30, 9:30 and 12:30 GMT) with determination coefficients yielding $r^2=0.42$, $r^2=0.88$ and $r^2=0.56$ respectively (Fig. 7d, e and f). Results, therefore, indicate that PRI was able to track diurnal changes in stomatal conductance as function of water stress condition from the airborne imager. More importantly, the lack of relationship found between stomatal conductance and structural and chlorophyll indices such as NDVI and TCARI/OSAVI suggested that changes observed in PRI were not due to structural effects of the water stress level.

The consistent relationships found between PRI and physiological indicators of water stress, Tc–Ta and stomatal
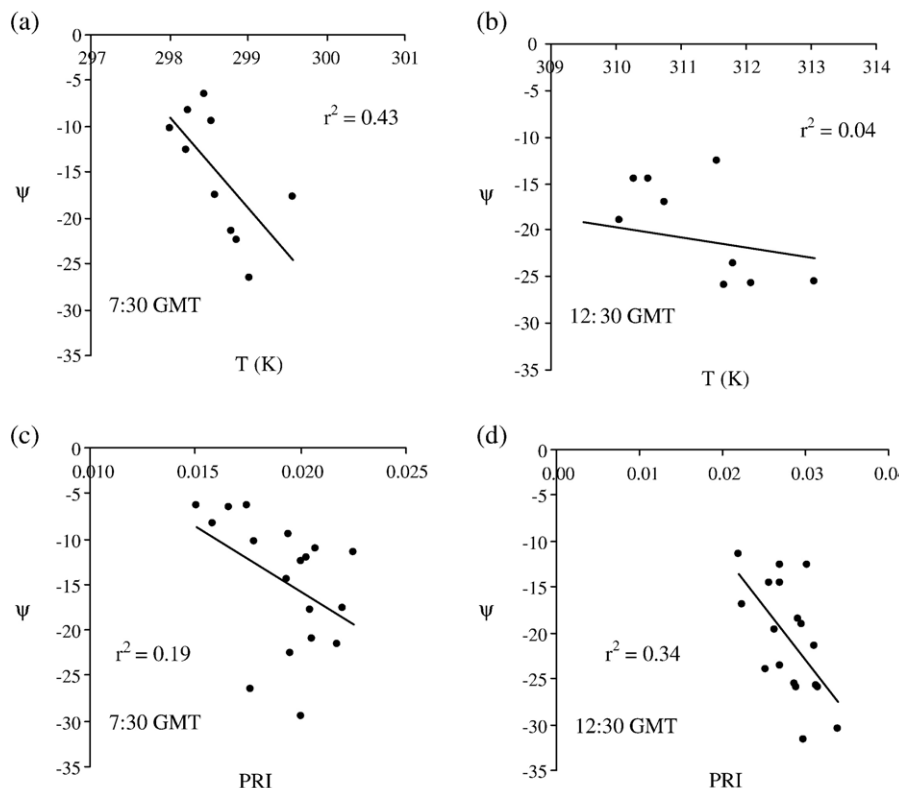

Fig. 9. Relationships between stem water potential and crown temperature at 7:30 (a) and 12:30 (b) GMT. Relationships between stem water potential and PRI at the same times (c and d).

conductance, was assessed against stem water potential, a precise indicator of the plant water status for predicting effects of water deficits on crop yields. As discussed in Sepulcre-Cantó et al. (2007), small changes in the relative water content of leaf tissues corresponds to large changes in leaf water potential (Acevedo et al., 1979; Kramer & Boyer, 1995). Therefore, although leaf water content may be easily detectable with remote sensing methods, it occurs at advanced stages of dehydration, and therefore represents a parameter of limited interest for predicting crop water status. Relationships found in this study between stem water potential and reflectance indices demonstrate the sensitivity of PRI as function of water stress condition (r^2=0.7 at a block level, Fig. 8a) with low sensitivity observed for indices such as NDVI (r^2=0.28, Fig. 8b) and TCARI/OSAVI (r^2=0.07, Fig. 8c). This result is consistent with the previous relationships found for PRI with Tc−Ta and G. Moreover, an additional analysis was conducted to assess the sensitivity of crown temperature and PRI with stem water potential as function of the time of day. Previous studies by Sepulcre-Cantó et al. (2006, 2007) demonstrated the sensitivity of crown temperature with field-measured water potential. Nevertheless, such studies demonstrated that crown temperature was better related with water potential early in the morning, suggesting that soil thermal effects near midday affected the correct retrieval of crown temperature. The thermal effects of adjacent soil pixels in non-homogeneous canopies, with mean temperature differences between tree crowns and sunlit soil of 11 K at 9:30 GMT and 23 K at 12:30 (this study) would affect correct retrieval of crown temperature and therefore the relation-

ships between temperature and water potential. The assessment conducted for all the instrumented crowns under study in this experiment (Fig. 9), demonstrates that in early morning (7:30 GMT) (Fig. 9a,c), stem water potential is better correlated with temperature (r^2=0.43) than with PRI (r^2=0.19). At midday (12:30 GMT) (Fig. 9b,d), with large thermal effects of adjacent bare soil pixels on the retrieved crown temperature, PRI was demonstrated to better track stem water potential (r^2=0.34) than temperature (r^2=0.04).

Finally, an assessment was conducted to study the relationship between ground-measured steady-state chlorophyll fluorescence (Ft) and image-derived indices and surface temperature. The hypothesis under assessment was that image PRI should be related with field-measured Ft at some degree level, while structural image-derived indices should not be sensitive to fluorescence effects of water stress. Results obtained at 12:30 GMT at tree scale (2004) are shown in Fig. 10, yielding r^2=0.54 for PRI (Fig. 10b), while NDVI and TCARI/OSAVI indices consistently yielded lower determination coefficients (r^2=0.22 and r^2=0.17, respectively) (Fig. 10a, c). Leaf-level measured Ft and image derived Tc−Ta showed a consistent relationship at tree level at 12:30 GMT (r^2=0.45; Fig. 10d).

3.2. Model simulation with FLIGHT

The FLIGHT model was used to simulate the viewing geometry and canopy architecture for the study site used in this
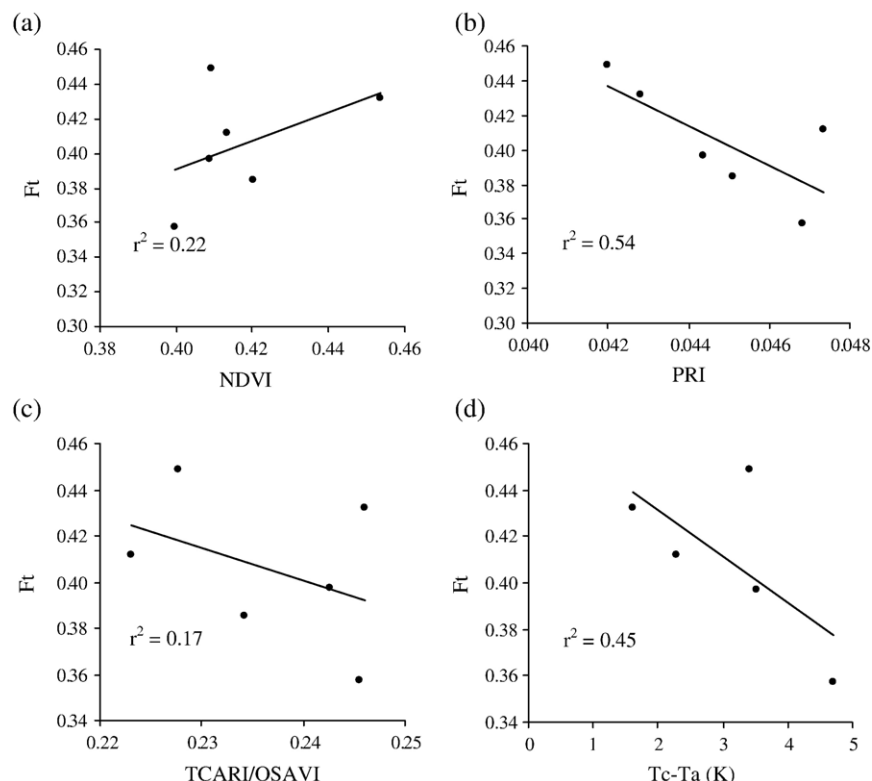
Fig. 10. Relationships obtained between NDVI, PRI, and TCARI/OSAVI with steady-state fluorescence (Ft) at the tree level at 12:30 (a, b and c respectively). Relationship between Ft and Tc−Ta at the same time for individual trees.
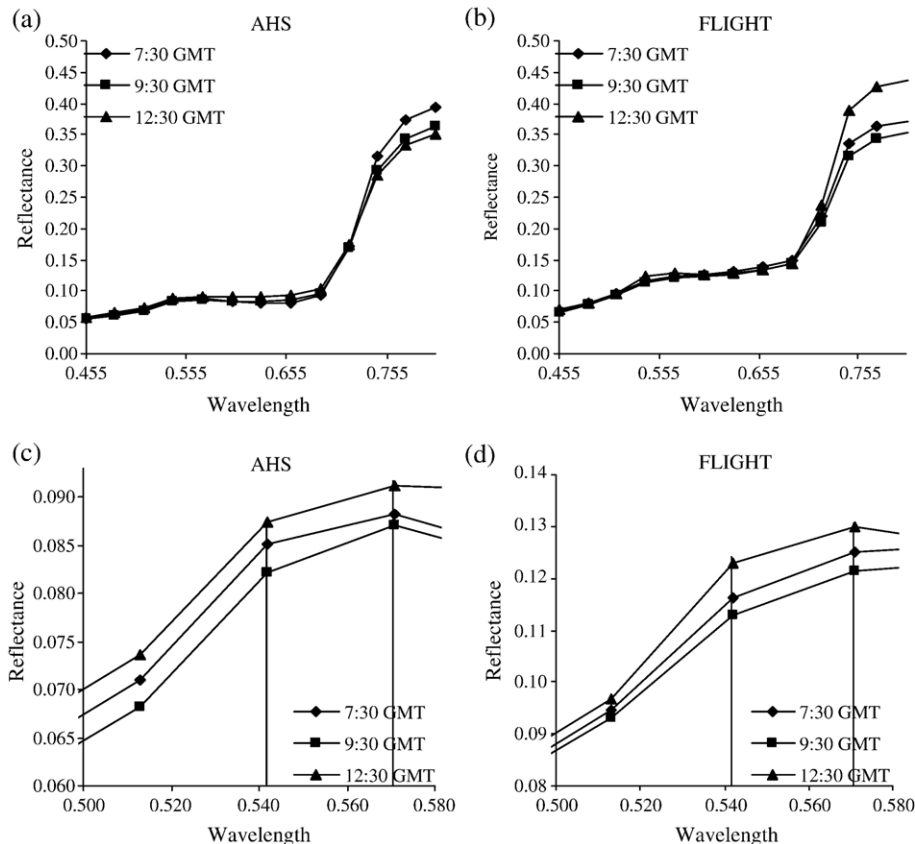
Fig. 11. AHS spectra extracted from pure crowns at the three acquisition times (a) and spectra simulated from FLIGHT (b) for three viewing geometries. Spectra in the 500–580 nm region used to calculate PRI (c and d).
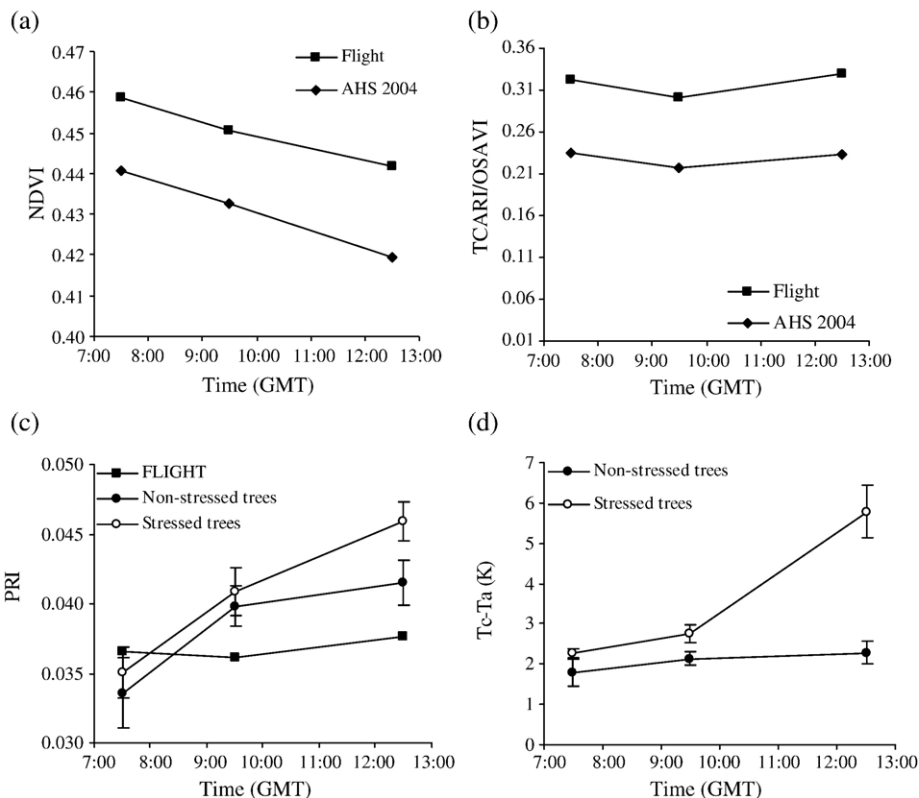

Fig. 12. Comparison between the vegetation indices calculated from AHS imagery and the FLIGHT simulations for NDVI (a), TCARI/OSAVI (b), and PRI (c), observing trend differences between PRI for stressed and non-stressed crowns (c) as compared with temperature changes for the same trees over the diurnal cycle (d).
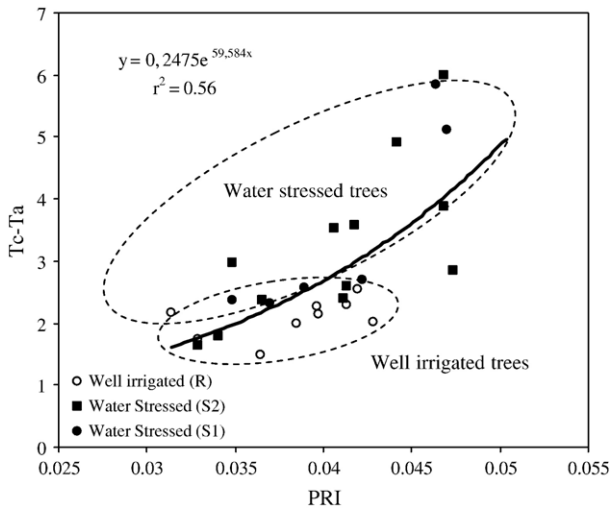
Fig. 13. Diurnal variation of Tc–Ta and PRI for stressed and non-stressed trees, enabling the identification of water stress levels over the course of the diurnal experiment.

study, and then the radiative transfer in that scene. The main objective was to assess BRDF effects on the vegetation indices used to track water stress, specifically PRI, therefore investigating the simulated trend of the PRI bands against the actual observed changes in the reflectance bands over the course of the diurnal experiment. The FLIGHT model was therefore used to simulate three scene configurations, corresponding to each image acquisition for the two years of the experiment (7:30, 9:30 and 12:30 GMT). The 3D scenes corresponding to each airborne overpass (Fig. 5a,c,e) were intended to mimic the exact plane attitude, including plane heading and the flight plan designed to fly on the solar plane. The main changes observed in the 3D scene simulations correspond to changes in the crop grid orientation against the solar plane, and the shadows cast by the trees as function of the sun angle (Fig. 5b,d,f). As expected, simulated scenes with FLIGHT show larger shadows at earlier times (7.30 GMT), almost disappearing at 12:30 GMT when the sun is at the zenith. Within-crown BRDF effects could then be assessed to study if the diurnal changes of the image-extracted indices were the main driver for the observed relationships with field-measured physiological parameters. The comparison between the spectra
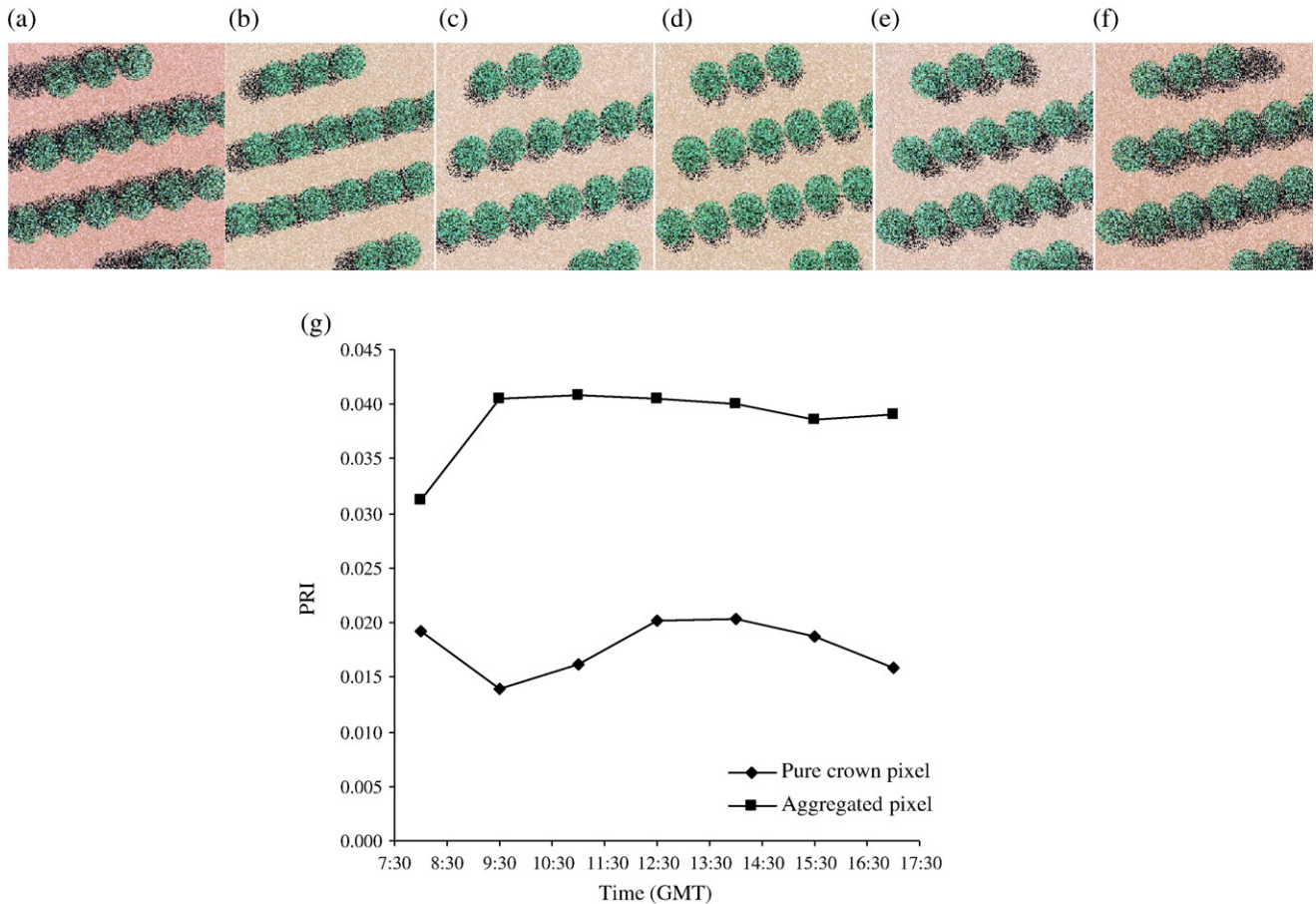

Fig. 14. Model simulations conducted with FLIGHT for the orchard scene at different times of day from 9:30 GMT to 17:00 GMT (a to f). Input parameters were: total LAI=0.393, fractional cover=0.393, crown LAI=1, leaf size=1.26, fraction of green leaves=0.85, fraction of bark=0, LAD=spherical, crown shape=spherical, crown radius=1.75 m, tree height=3.45 m, soil roughness=0, aerosol optical thickness=0.1, view zenith=0°, view azimuth=0°, solar zenith=53.6° (a), 36.1° (b), 21.5° (c), 19.6° (d), 32.7° (e) and 49.9° (f), solar azimuth=92.4° (a), 109.7° (b), 143.2° (c), 205.6° (d), 245.3° (e) and 264.4° (f). PRI values corresponding to the simulations along the day are presented in (g) for pure crown pixels and aggregated pixels.

extracted from pure crowns on the airborne imagery at three acquisition times (Fig. 11a) and the simulated spectra using the FLIGHT model for the three viewing geometries (Fig. 11b) shows a consistent agreement in BRDF effects at the 500–600 nm spectral range (Fig. 11c and d), the region used for the calculation of the PRI index.

The three vegetation indices used in this study, NDVI, TCARI/OSAVI and PRI were calculated from the simulated spectra for the three acquisition times. A comparison between the diurnal trend of the vegetation indices and the diurnal trend of the simulations for pure crowns was conducted. Diurnal changes in NDVI (Fig. 12a) and TCARI/OSAVI (Fig. 12b) follow the same trend for both image-extracted and model simulated indices, therefore showing consistent diurnal effects caused by BRDF on the crown reflectance. However, diurnal changes in PRI (Fig. 12c) show a different trend for the simulated and image-extracted index, supporting the hypothesis that PRI is affected by both BRDF and absorption changes in xanthophyll pigments caused by diurnal water stress changes. Moreover, a different trend in canopy PRI is observed for water stressed and non-stressed trees, which increases at the time of maximum stress (12:30 GMT) (Fig. 12c). Differences observed in the PRI trend for stressed and non-stressed trees acquired with airborne imagery is consistent with the measured trend for Tc–Ta for the same times and measured trees (Fig. 12d), exhibiting an increasing difference in crown temperature for stressed trees as compared with well-irrigated trees. This experiment demonstrates that the

images acquired for two years show a consistent diurnal trend change for PRI, probably due to effects of the xanthophyll cycle pigment change function of the water stress levels. The diurnal variation of PRI against Tc–Ta for the monitored trees ($r^2 = 0.56$, Fig. 13) show that well-irrigated trees (R treatment, full ET) remain in the lower left portion of the relationship, showing lower PRI and Tc–Ta values over the course of the diurnal cycle. Water stressed trees (S1 and S2 treatments) show an increment on both PRI and Tc–Ta over the course of the diurnal experiment. These results demonstrate the potential use of a reflective index combined with crown temperature to assess water stress levels over diurnal cycles.

A further study was conducted with FLIGHT to assess the effects of sun angle, soil reflectance, and LAI on the PRI index calculated from pure crown reflectance and aggregated pixels. The objective was to investigate the potential undesired BRDF effects on the index used for both temporal and spatial studies with high- and medium-resolution imagery. Fig. 14 shows a 3D scene for sun zenith angles ranging between 19.6° and 53.6°, with azimuth angles ranging between 92.4° and 264.4° (Fig. 14a to f), including the effects of shadows on the canopy reflectance. With a canopy configuration comprising a scene LAI=0.393, fractional cover=0.39, crown LAI=1, LAD = spherical, and a spherical crown shape, simulation results show that PRI is affected by BRDF effects as function of sun angle changes over the course of the day (Fig. 14g). As expected, background effects on PRI were clearly detectable, as seen in the simulation results from
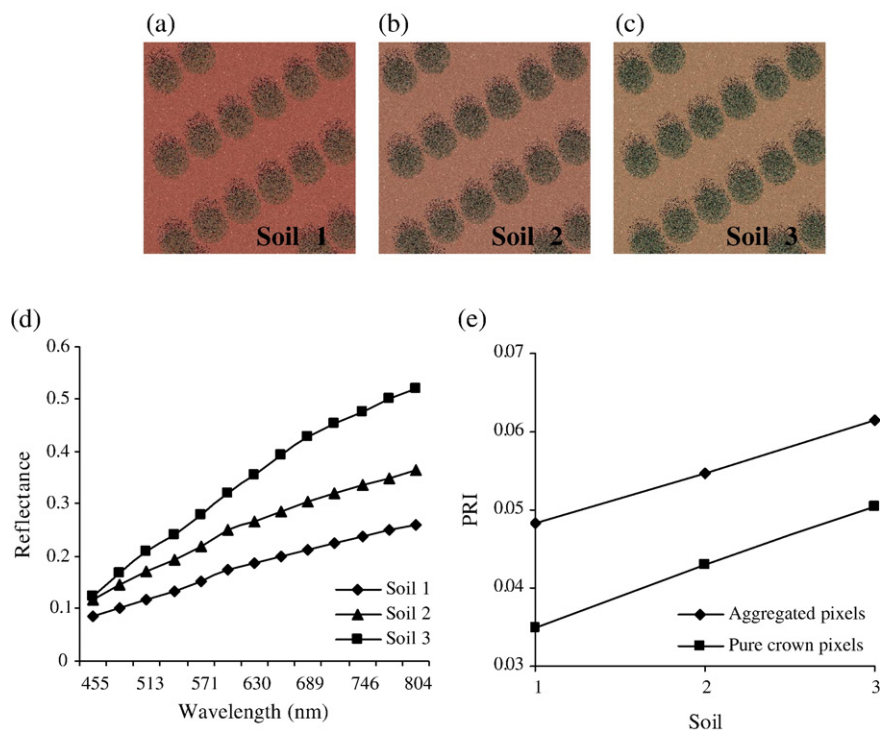

Fig. 15. Model simulations conducted with FLIGHT for the orchard scene with different soil types (a to c, spectra shown in d). Input parameters were: total LAI=0.449, fractional cover=0.449, crown LAI=1, leaf size=1.26, fraction of green leaves=0.85, fraction of bark=0, LAD=spherical, crown shape=spherical, crown radius=1.75 m, tree height=3.45 m, soil roughness=0, aerosol optical thickness=0.1, view zenith=0°, view azimuth=0°, solar zenith=21.36°, solar azimuth=20.94°. The input soil spectra were acquired from the AHS imagery (spectra presented in (d)) and changed for each simulation. The effect of the different soil types (1, 2 and 3) on PRI is presented in (e) for pure crown pixels and aggregated pixels.
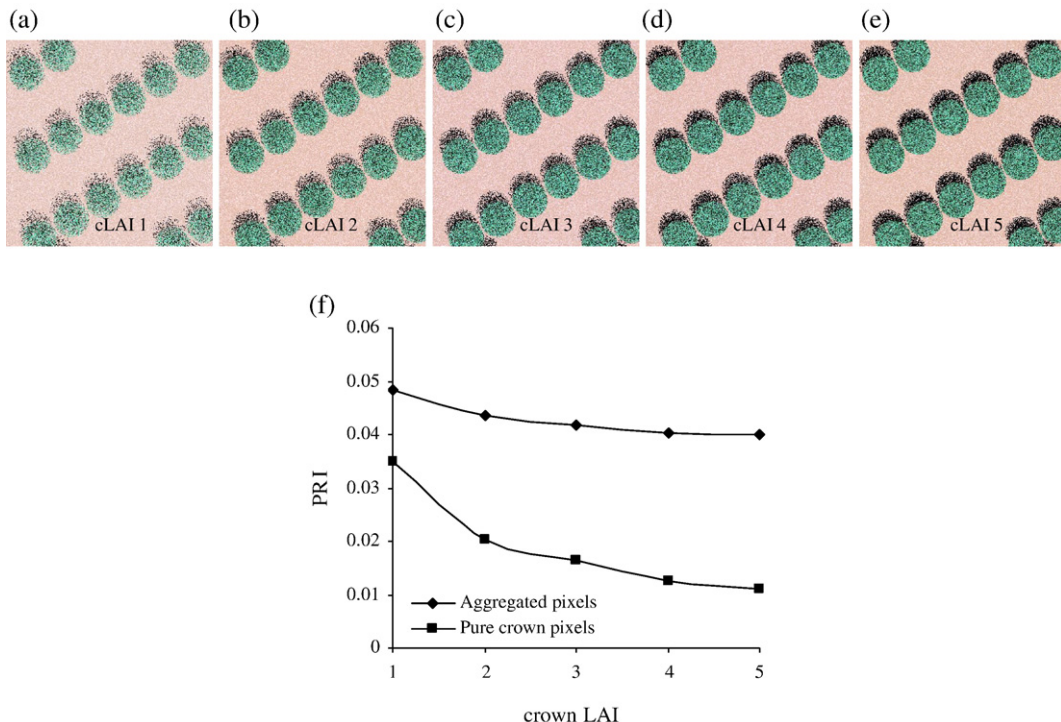
Fig. 16. Model simulations conducted with FLIGHT for the orchard scene as function of crown LAI variation. Input parameters were: total LAI=0.449 (a), 0.898 (b), 1.347 (c), 1.796 (d), 2.255 (e), fractional cover=0.449, crown LAI=1, 2, 3, 4, 5 (respectively), leaf size=1.26, fraction of green leaves=0.85, fraction of bark=0, LAD=1, crown shape=spherical, crown radius=1.75 m, tree height=3.45 m, soil roughness=0, aerosol optical thickness=0.15, view zenith=0°, view azimuth=0°, solar zenith=21.36°, solar azimuth=20.94°. PRI as function of crown LAI is presented in (f) for pure crown pixels and aggregated pixels.

aggregated pixels and pure crown reflectance as function of the viewing geometry. The assessment of background effects on simulated PRI was studied as function of different soil spectra acquired with the airborne sensor used in this study (Fig. 15). Three scene configurations were simulated (Fig. 15a b c) corresponding with three soil spectra (Fig. 15d), and PRI calculated for pure crowns and the entire scene aggregating pure crown, soil and shadow effects (Fig. 15e). The simulation results with a scene LAI=0.449, fractional cover=0.45, crown LAI=1, spherical LAD, and a spherical crown shape suggest that large effects on PRI occur as function of the soil background even for pure crown components. Effects due to the component aggregation (crown+soil+shadows) as acquired from medium-resolution sensors are also observable. These results are especially important when conducting spatial assessments of the PRI index in low LAI canopies. The simulated variation in PRI for the three soil spectra in targeted crowns ranged from 0.035 to 0.05, due to soil background effects on the index. The range of variation for PRI in the simulation is the same as that obtained as function of water stress effects (Fig. 13); this implies that a careful assessment needs to be conducted when performing spatial analyses of PRI due to the potentially large background effects on PRI which could be incorrectly attributed to stress levels. Finally, the effects of scene LAI were assessed for a range between LAI=0.5 and LAI=2.2 (Fig. 16a b c d e) considering a fractional cover=0.5, crown LAI ranging between 1 and 5, spherical LAD, and crown spherical shape. Simulation results for crown pixels and aggregated components (Fig. 16f) shows large variations on

PRI as function of LAI variation. LAI effects on PRI at the crown level are critical, and could be incorrectly attributed to stress condition, with a decreasing trend on PRI as LAI increases. The simulations conducted to assess the effects of the viewing geometry, background and LAI on crown and scene PRI demonstrates that they need to be seriously considered when generating spatial maps of PRI from airborne and satellite imagery to assess vegetation condition.

4. Conclusions

The diurnal airborne campaigns conducted for two years over an experimental crop field demonstrate that the airborne-level PRI index is sensitive to the de-epoxidation of the xanthophyll pigment cycle caused by water stress levels under deficit irrigation. Among the three vegetation indices calculated from the airborne imagery at 2 m spatial resolution, PRI, TCARI/OSAVI, as an indicator of chlorophyll a+b concentration, and NDVI, used to track structural changes on the canopy, only airborne PRI demonstrated sensitivity to diurnal changes in physiological indicators of water stress, such as canopy temperature minus air temperature (Tc–Ta), stomatal conductance (G), and stem water potential (ψ) measured in the field at each time of image acquisition. No relationships were found over the diurnal experiment between NDVI and TCARI/OSAVI with tree-measured physiological measures. Moreover, a relationship was also found between leaf-level steady-state fluorescence (Fs) and image PRI calculated from the same trees

monitored over the course of the diurnal flight campaigns. The 2 m spatial resolution imagery acquired three times over the course of the day with the AHS sensor enabled targeting crowns and extracting image based information in the VIS-NIR region for vegetation index calculation, as well as in the thermal region for crown temperature monitoring.

The effects of the bi-directional reflectance distribution function changes in the vegetation indices used in this study were simulated with the 3D FLIGHT canopy reflectance model linked with PROSPECT leaf model. AHS reflectance spectra were compared with those from model-simulated scenes that accounted for the viewing geometry configuration as function of the airborne acquisitions conducted on the solar plane. Diurnal trends in the airborne vegetation indices demonstrate that NDVI and TCARI/OSAVI are well simulated by crown-level simulations with FLIGHT, capturing the BRDF changes associated with the sun angle changes. On the other hand, the canopy model did not simulate correctly the image-observed diurnal changes in PRI, demonstrating that PRI bands are affected diurnally by the confounding effects of BRDF effects and the absorption changes due to the de-epoxidation of the xanthophyll pigment function of water stress. Moreover, differences observed in diurnal crown PRI for well-watered and water-stressed trees at mid-day depression agree with diurnal trends on Tc−Ta at the same times. These results confirm that diurnal changes observed in PRI are both structurally and physiologically driven, and not only affected by BRDF. A relationship obtained between Tc−Ta (thermal region) and PRI (reflective region) for single days enabled the identification of trees under water stress. Well watered trees remained with low Tc−Ta and PRI values over the course of the day, while stressed trees increased their temperature and PRI.

The simulation assessment on the effects on PRI as function of sun angle, soil background, and crown LAI demonstrate that PRI is highly affected by the canopy structure and background. Changes in PRI as function of canopy LAI are comparable to those found as function of water stress levels. Therefore a careful assessment of canopy structure variability needs to be conducted when PRI is used to study the spatial distribution of vegetation stress. Soil background and canopy LAI are key factors to account for when PRI is used to detect water stress.

Acknowledgements

References

Acevedo, E., Fereres, E., Hsiao, T., & Henderson, D. (1979). Diurnal growth trends, water potential, and osmotic adjustment of maize and sorghum leaves in the field. *Plant Physiology*, 64, 476−480.

Asner, G. P., Carlson, K. M., & Martin, R. E. (2005). Substrate age and precipitation effects on Hawaiian forest canopies from spaceborne imaging spectroscopy. *Remote Sensing of Environment*, 98, 457−467.

Barton, C. V. M., & North, P. R. J. (2001). Remote Sensing of canopy light use efficiency using the Photochemical Reflectance Index. Model and analysis. *Remote Sensing of Environment*, 78(264), 273.

Ben-Dor, E., & Levin, N. (2000). Determination of surface reflectance from raw hyperspectral data without simultaneous ground data measurements: A case study of the GER 63-channel sensor data acquired over Naan, Israel. *International Journal of Remote Sensing*, 21, 2053−2074.

Berk, A., Anderson, G. P., Acharya, P. K., Chetwynd, J. H., Bernstein, L. S., Shettle, E. P., et al. (1999). *MODTRAN4 user's manual*. Hanscom AFB, MA: Air Force Research Laboratory.

Daughtry, C. S. T., Walthall, C. L., Kim, M. S., Brown de Colstoun, E., & McMurtrey, J. E., III (2000). Estimating corn leaf chlorophyll concentration from leaf and canopy reflectance. *Remote Sensing of Environment*, 74, 229−239.

Disney, M. I., Lewis, P., & North, P. R. J. (1999). Montecarlo ray tracing in optical canopy reflectance modelling. *Remote Sensing Reviews*, 18(2−4), 197−226.

Dobrowsky, S. Z., Pushnik, J. C., Zarco-Tejada, P. J., & Ustin, S. L. (2005). Simple reflectance indices track heat and water stress-induced changes in steady-state chlorophyll fluorescence at the canopy scale. *Remote Sensing of Environment*, 97, 403−414.

Drolet, G. G., Huemmrich, K. F., Hall, F. G., Middleton, E. M., Black, T. A., Barr, A. G., et al. (2005). A MODIS-derived Photochemical Reflectance Index to detect inter-annual variations in the photosynthetic light-use efficiency of a boreal deciduous forest. *Remote Sensing of Environment*, 98, 212−224.

Evain, S., Flexas, J., & Moya, I. (2004). A new instrument for passive remote sensing: 2. Measurement of leaf and canopy reflectance changes at 531 nm and their relationship with photosynthesis and chlorophyll fluorescence. *Remote Sensing of Environment*, 91, 175−185.

Filella, I., Amaro, T., Araus, J. L., & Peñuelas, J. (1996). Relationship between photosynthetic radiation-use efficiency of barley canopies and the Photochemical Reflectance Index (PRI). *Physiologia Plantarum*, 96, 211−216.

Filella, I., Peñuelas, J., Llorens, L., & Estiarte, M. (2004). Reflectance assessment of seasonal and annual changes in biomass and CO2 uptake of a Mediterranean shrubland submitted to experimental warming and drought. *Remote Sensing of Environment*, 90, 308−318.

Fuentes, D. A., Gamon, J. A., Cheng, Y., Claudio, H. C., Qiu, H. L., Mao, Z., et al. (2006). Mapping carbon and water vapour fluxes in a chaparral ecosystem using vegetation indices derived from AVIRIS. *Remote Sensing of Environment*, 103, 312−323.

Gamon, J. A., Peñuelas, J., & Field, C. B. (1992). A narrow-wave band spectral index that track diurnal changes in photosynthetic efficiency. *Remote Sensing of Environment*, 41, 35−44.

Gamon, J. A., Serrano, L., & Surfus, J. S. (1997). The Photochemical Reflectance Index: An optical indicator of photosynthetic radiation use efficiency across species, functional types and nutrient levels. *Oecologia*, 112, 492−501.

Gamon, J. A., & Surfus, J. S. (1999). Assessing leaf pigment content and activity with a reflectometer. *New Phytologist*, 143, 105−117.

Goel, N. S., & Thompson, R. L. (2000). A snapshot of canopy reflectance models and a universal model for the radiation regime. *Remote Sensing Reviews*, 18(2), 197−225.

Guo, J., & Trotter, C. M. (2004). Estimating photosynthetic light-use efficiency using the Photochemical Reflectance Index: Variations among species. *Functional Plant Biology*, 31, 255−565.

Haboudane, D., Miller, J. R., Pattey, E., Zarco-Tejada, P. J., & Strachan, I. (2004). Hyperspectral vegetation indices and novel algorithms for predicting green LAI of crop canopies: Modeling and validation in the context of precision agriculture. *Remote Sensing of Environment*, 90(3), 337−352.

Haboudane, D., Miller, J. R., Tremblay, N., Zarco-Tejada, P. J., & Dextraze, L. (2002). Integrated narrow-band vegetation indices for prediction of crop

chlorophyll content for application to precision agriculture. *Remote Sensing of Environment*, *84*(2–3), 416−426.

Idso, S. B., Jackson, R. D., & Reginato, R. J. (1978). Extending the "degree day" concept of phenomenological development to include water stress effects. *Ecology*, *59*, 431−433.

Jackson, R. D., Idso, S. B., Reginato, R. J., & Ehrier, W. L. (1977). Crop temperature reveals stress. *Crop Soils*, *29*, 10−13.

Jackson, R. D., & Pinter, P. J., Jr. (1981). Detection of water stress in wheat by measurement of reflected solar and emitted thermal IR radiation. *Spectral signatures of objects in remote sensing* (pp. 399−406). Versalles, France: Institut National de la Reserche Agronomique.

Koetz, B., Baret, F., Poilvé, H., & Hill, J. (2005). Use of coupled canopy structure dynamic and radiative transfer models to estimate biophysical canopy characteristics. *Remote Sensing of Environment*, *95*(1), 115−124.

Kramer, P. J., & Boyer, J. S. (1995). *Water relations of plants and soils.* San Diego, CA, USA: Academic Press.

Louis, J., Ounis, A., Ducruet, J. M., Evain, S., Laurila, T., Thum, T., et al. (2005). Remote Sensing of sunlight-induced chlorophyll fluorescence and reflectance of Scots pine in the boreal forest during spring recovery. *Remote Sensing of Environment*, *96*, 37−48.

Mariscal, M. J., Orgaz, F., & Villalobos, F. J. (2000). Modelling and measurement of radiation interception by olive canopies. *Agricultural and Forest Meteorology*, *100*, 183−197.

Nakaji, T., Oguma, H., & Fujinuma, Y. (2006). *International Journal of Remote Sensing*, *27*(3), 493−509.

Nichol, C. J., Huemmrich, K. F., Black, T. A., Jarvis, P. G., Walthall, J. G., & Hall, F. G. (2000). Remote sensing of photosynthetic-light-use efficiency of boreal forest. *Agricultural and Forest Meteorology*, *101*, 131−142.

Nichol, C. J., Lloyd, J., Shibistova, O., Arneth, A., Röser, C., Knohl, A., et al. (2002). Remote sensing of photosynthetic-light-use-efficiency of a Siberian boreal forest. *Tellus*, *54B*, 677−687.

Nichol, C. J., Rascher, U., Matsubara, S., & Osmond, B. (2006). Assessing photosynthetic efficiency in an experimental mangrove canopy using remote sensing and chlorophyll fluorescence. *Trees*, *20*, 9−15.

North, P. R. J. (1996). Three-dimensional forest light interaction model using a Montecarlo method. *IEEE Transactions on Geosciences and Remote Sensing*, *34*(5), 946−956.

Peñuelas, J., Gamon, J. A., Fredeen, A. L., Merino, J., & Field, C. B. (1994). Reflectance indices associated with physiological changes in nitrogen- and water-limited sunflower leaves. *Remote Sensing of Environment*, *48*, 135−146.

Peñuelas, J., & Inoue, Y. (2000). Reflectance assessment of canopy CO_2 uptake. *International Journal of Remote Sensing*, *21*, 3353−3356.

Pérez-Priego, O., Zarco-Tejada, P. J., Sepulcre-Cantó, G., Miller, J. R., & Fereres, E. (2005). Detection of water stress in orchard trees with a high-resolution spectrometer through chlorophyll fluorescence *in-filling* of the O_2−A band. *IEEE Transactions on Geoscience and Remote Sensing*, *43*, 2860−2869.

Rahman, A. F., Cordova, V. D., Gamon, J. A., Schmid, H. P., & Sims, D. A. (2004). Potential of MODIS ocean bands for estimating CO_2 flux from terrestrial vegetation: A novel approach. *Geophysical Research Letters*, *31*.

Richardson, A. D., & Berlyn, G. P. (2002). Spectral reflectance and photosynthetic properties of *Betula papyrifera* (Betulaceae) leaves along an elevational gradient on Mt. Mansfield, Vermont, USA. *American Journal of Botany*, *89*(1), 88−94.

Richardson, A. D., Berlyn, G. P., & Duigan, S. P. (2003). Reflectance of Alaskan black spruce foliage in relation to elevation and latitude. *Tree Physiology*, *23*, 537−544.

Rondeaux, G., Steven, M., & Baret, F. (1996). Optimization of soil-adjusted vegetation indices. *Remote Sensing of Environment*, *55*(2), 95−107.

Rouse, J. (1974). *Monitoring the vernal advancement and retrogradation (greenwave effect) of natural vegetation.*

Sepulcre-Cantó, G., Zarco-Tejada, P. J., Jiménez-Muñoz, J. C., Sobrino, J. A., de Miguel, E., & Villalobos, F. J. (2006). Within-field thermal variability detection as function of water stress in *Olea europaea* L. orchards with high spatial remote sensing imagery. *Agricultural and Forest Meteorology*, *136*, 31−44.

Sepulcre-Cantó, G., Zarco-Tejada, P. J., Jiménez-Muñoz, J. C., Sobrino, J. A., Soriano, M. A., Fereres, E., et al. (2007 April 12). Monitoring yield and fruit quality parameters in open-canopy tree crops under water stress. Implications for ASTER. *Remote Sensing of Environment*, *107*(3), 455−470.

Serrano, L., & Peñuelas, J. (2005). Assessing forest structure and function from spectral transmittance measurements: A case study in a Mediterranean holm oak forest. *Tree Physiology*, *25*, 67−74.

Sims, D. A., & Gamon, J. A. (2002). Relationships between leaf pigment content and spectral reflectance across a wide range of species, leaf structures and developmental stages. *Remote Sensing of Environment*, *81*, 337−354.

Sims, D. A., Luo, H., Hastings, S., Oechel, W. C., Rahman, A. F., & Gamon, J. A. (2006). Parallel adjustment in vegetation greenness and ecosystem CO2 exchange in response to drought in a Southern California chaparral ecosystem. *Remote Sensing of Environment*, *103*, 289−303.

Sobrino, J. A., Jiménez-Muñoz, J. C., Zarco-Tejada, P. J., Sepulcre-Cantó, G., & de Miguel, E. (2006). Land surface temperature derived from airborne hyperspectral scanner thermal infrared data. *Remote Sensing of Environment*, *102*, 99−115.

Strachan, I. B., Pattey, E., & Boisvert, J. B. (2002). Impact of nitrogen and environmental conditions on corn as detected by hyperspectral reflectance. *Remote Sensing of Environment*, *80*, 213−224.

Stylinski, C. D., Gamon, J. A., & Oechel, W. C. (2002). Seasonal patterns of reflectance indices, carotenoid pigments and photosynthesis of evergreen chaparral species. *Oecologia*, *131*, 366−374.

Tambussi, E. A., Casadesus, J., Munne-Bosch, S. M., & Araus, J. L. (2002). Photoprotection in water-stressed plants of durum wheat (*Triticum turgidum* var. *durum*): Changes in chlorophyll fluorescence, spectral signature and photosynthetic pigments. *Functional Plant Biology*, *29*, 35−44.

Thenot, F., Méthy, M., & Winkel, T. (2002). The Photochemical Reflectance Index (PRI) as a water-stress index. *International Journal of Remote Sensing*, *23*(23), 5135−5139.

Trotter, G. M., Whitehead, D., & Pinkney, E. J. (2002). The Photochemical Reflectance Index as a measure of photosynthetic light use efficiency for plants with varying foliar nitrogen contents. *International Journal of Remote Sensing*, *23*(6), 1207−1212.

Weng, G. H., Chen, Y. N., & Liao, T. S. (2006). Relationships between chlorophyll fluorescence parameters and Photochemical Reflectance Index of tree species adapted to different temperature regimes. *Functional Plant Biology*, *33*, 241−246.

Weng, J. H., Liao, T. S., Hwang, M. Y., Chung, C. C., Lin, C. P., & Chu, C. H. (2006). Seasonal variation in photosystem II efficiency and Photochemical Reflectance Index of evergreen trees and perennial grasses growing at low and high elevations in subtropical Taiwan. *Tree Physiology*, *26*, 1097−1104.

Whitehead, D., Boelman, N. T., Turnbull, M. H., Griffin, K. L., Tissue, D. T., Barbour, M. M., et al. (2005). Photosynthesis and reflectance indices for rainforest species in ecosystems undergoing progression along a soil fertility chronosequence in New Zealand. *Oecologia*, *144*, 233−244.

Winkel, T., Méthy, M., & Thénot, F. (2002). Radiation use efficiency, chlorophyll fluorescence , and reflectance indices associated with ontogenic changes in water-limited *Chenopodium quinoa* leaves. *Photosynthetica*, *40* (2), 227−232.

Zarco-Tejada, P. J., Berjón, A., López-Lozano, R., Miller, J. R., Martín, P., Cachorro, V., et al. (2005). Assessing vineyard condition with hyperspectral indices: Leaf and Canopy reflectance simulation in a row-structured discontinuous canopy. *Remote Sensing of Environment*, *99*, 271−287.

Zarco-Tejada, P. J., Miller, J. R., Mohammed, G. H., & Noland, T. L. (2000). Chlorophyll fluorescence effects on vegetation apparent reflectance: I. Leaf-level measurements and model simulation. *Remote Sensing of Environment*, *74*(3), 582−595.

Zarco-Tejada, P. J., Miller, J. R., Morales, A., Berjón, A., & Agüera, J. (2004). Hyperspectral indices and model simulation for chlorophyll estimation in open-canopy tree crops. *Remote Sensing of Environment*, *90*(4), 463−476.